Gas Transfer in Cellularized Collagen-Membrane Gas Exchange Devices

Citation: Lo, Justin H., Erik K. Bassett, Elliot J. N. Penson, David M. Hoganson, and Joseph P. Vacanti. "Gas Transfer in Cellularized Collagen-Membrane Gas Exchange Devices." Tissue Engineering Part A 21, no. 15–16 (August 2015): 2147–2155. © 2015 Mary Ann Liebert, Inc.

As Published: http://dx.doi.org/10.1089/ten.TEA.2014.0369

Publisher: Mary Ann Liebert, Inc.

Persistent URL: http://hdl.handle.net/1721.1/98486

Version: Final published version: final published article, as it appeared in a journal, conference proceedings, or other formally published context

TISSUE ENGINEERING: Part A
Volume 21, Numbers 15 and 16, 2015

DOI: 10.1089/ten.tea.2014.0369

termis
Tissue Engineering
& Regenerative Medicine
International Society

ORIGINAL ARTICLE

Gas Transfer in Cellularized Collagen-Membrane Gas Exchange Devices

Justin H. Lo, PhD,[1–3] Erik K. Bassett, MS,[1] Elliot J. N. Penson, BS,[1]
David M. Hoganson, MD,[1] and Joseph P. Vacanti, MD[1,2]

Chronic lower respiratory disease is highly prevalent in the United States, and there remains a need for alternatives to lung transplant for patients who progress to end-stage lung disease. Portable or implantable gas oxygenators based on microfluidic technologies can address this need, provided they operate both efficiently and biocompatibly. Incorporating biomimetic materials into such devices can help replicate native gas exchange function and additionally support cellular components. In this work, we have developed microfluidic devices that enable blood gas exchange across ultra-thin collagen membranes (as thin as 2 μm). Endothelial, stromal, and parenchymal cells readily adhere to these membranes, and long-term culture with cellular components results in remodeling, reflected by reduced membrane thickness. Functionally, acellular collagen-membrane lung devices can mediate effective gas exchange up to $\sim$288 mL/min/m^2 of oxygen and $\sim$685 mL/min/m^2 of carbon dioxide, approaching the gas exchange efficiency noted in the native lung. Testing several configurations of lung devices to explore various physical parameters of the device design, we concluded that thinner membranes and longer gas exchange distances result in improved hemoglobin saturation and increases in pO_2. However, in the design space tested, these effects are relatively small compared to the improvement in overall oxygen and carbon dioxide transfer by increasing the blood flow rate. Finally, devices cultured with endothelial and parenchymal cells achieved similar gas exchange rates compared with acellular devices. Biomimetic blood oxygenator design opens the possibility of creating portable or implantable microfluidic devices that achieve efficient gas transfer while also maintaining physiologic conditions.

Introduction

Chronic lower respiratory diseases such as chronic obstructive pulmonary disease afflict over 5% of the U.S. population, leading to over 140,000 deaths annually.[1] For patients who progress to end-stage lung disease, lung transplantation remains the standard of care, yet 11% of patients who enter the U.S. lung transplant list die before transplantation, reflecting the dire shortage of organs.[2] Thus, there is a need for portable or implantable devices that assist with gas exchange in patients who are waiting for transplant, whose transplants are failing, or for whom transplant is contraindicated.

Existing gas-exchange support devices such as extracorporeal membrane oxygenation (ECMO) have been used clinically as respiratory support for patients whose conditions are refractory to mechanical ventilation.[3] However, due to bleeding risk associated with anticoagulation, risk of neurological complications, and need for continuous monitoring, ECMO is not viable outside of the hospital setting.[4] Recently, the Hemolung and Novalung have successfully bridged patients to transplant, but still require monitoring for thrombus formation.[5,6] Furthermore, these technologies are primarily useful in hypercapnic lung respiratory failure rather than hypoxemic conditions or those requiring full cardiopulmonary support.[3] Most of the complications associated with extracorporeal membrane ventilation are the direct or indirect consequence of unphysiologic blood flow in membrane cartridge and hollow fiber architectures, wherein blood passes through a large chamber bordered or traversed by bare or heparinized plastic air channels. Engineering lung assist devices with biomimetic materials, cellular components, and physiologic blood flow profiles can promote self-maintenance while reducing the risk of coagulation, enabling the use of such devices in long-term outpatient therapy.

[1]Department of Surgery, Center for Regenerative Medicine, Massachusetts General Hospital, Boston, Massachusetts.
[2]Harvard Medical School, Boston, Massachusetts.
[3]Harvard-MIT Division of Health Sciences and Technology, Cambridge, Massachusetts.

Broadly speaking, there are two approaches to creating next-generation lung assist devices and artificial lungs. The first strategy is to rationally design and fabricate networks of vascular and respiratory channels, typically using gas-permeable polymer materials such as polycarbonate or polydimethylsiloxane (PDMS).[7–10] This strategy has the advantages of gas exchange efficiency near that of the native lung, affording greater control of physical parameters, and in some cases not requiring any living components. However, introduction of extensive foreign material or operation under unsuitable hemodynamic flows and vessel geometries can sacrifice biocompatibility and promote life-threatening thrombosis.

The second general strategy is to establish or isolate ECM-based environments and seed these with cells that self-pattern and differentiate into mature lung structures.[11–14] Seeding of collagen and other extracellular matrix (ECM)-inspired scaffolds has yielded epithelial and Type II pneumocyte-like cells in alveolus-like configurations; however, these efforts have not to date been tested for gas exchange function.[12] Decellularized rat lungs have been used as natural ECM scaffolds, and when repopulated with epithelial and endothelial cells, can be transplanted orthotopically and maintain function for several hours.[13,14] The decellularized lung scaffold approach, more recently demonstrated in nonhuman primates to promote reseeding by mesenchymal stem cells,[15] creates artificial lungs that are grossly and histologically lung-like. Nevertheless, physical constraints inherent from the scaffold limit both modularity and the engineering tools available to ensure continuous function and maintenance.

Acknowledging the strengths of each approach above, we employed a hybrid construction in which a planned, fabricated network is composed of materials amenable to sustaining cellular components. Specifically, we present a prototypic biomimetic lung assist device based on gas exchange across an ultra-thin collagen membrane, with blood flowing in microfabricated vascular networks developed previously by our group.[16] We have tested such devices in acellular configurations and after population of the membrane with parenchymal and endothelial cells. Endothelial cells have been shown in the literature to reduce thrombogenicity of a synthetic gas exchange membrane,[17] and we believe that integrating these cells with a collagen membrane and parenchymal cells further enables plasticity and sustainability of the system. Since the collagen film functions analogously to the basement membrane between pneumocytes and endothelial cells in the physiologic setting, such a device has potential to facilitate efficient gas exchange while maintaining a biocompatible environment.

Materials and Methods

Overview of devices

Two types of microfluidic devices were designed and manufactured in this work: preliminary work used single-channel transwell devices (Supplementary Fig. S1; Supplementary Data are available online at www.liebertpub.com/tea), and subsequent iterations used multi-channel collagen-membrane gas exchange devices (all other figures). In both models, blood flowing in vascular channels was separated from an upper air chamber by a thin collagen membrane, but the techniques for manufacture and gas exchange testing differ.

Manufacture and gas exchange testing of single-channel transwell devices

A thin collagen membrane (45 μm thick) was created by air-drying a slurry of fibrillar bovine collagen. The collagen membrane was dehydrothermally cross-linked, then sterilized with ethylene oxide. To create the single-channel model, the collagen membrane was mounted in the place of the standard membrane in a 24-well plate transwell. Transwells with a polycarbonate membrane of 0.4 μm pore size and 10 μm thickness were used as controls.

Human umbilical vein endothelial cells (HUVECs) were seeded on the bottom of the collagen or polycarbonate membranes of the transwells and Human Type II pneumocytes (H441 cell line) were seeded on the top side ($n=3$ for both collagen and control membranes). In controls, the bottom of the collagen membrane was seeded with HUVECs or fibroblasts (NIH-3T3 cell line) ($n=3$ for both cell types). Cell were cultured under standard conditions for 2 weeks.

Devices were assembled by affixing the transwell to the PDMS (Sylgard 184; Dow Corning) layers, with the membrane forming the top wall of the single 250 μm-deep vascular channel and air filling the transwell chamber above the membrane, as depicted in Supplementary Figure S1A. Computational fluid dynamics analysis was performed using COSMOSFloWorks™ (SolidWorks) to evaluate the device, estimating pressures on the order of 1 mmHg in the air chamber and 10 mmHg in the channel. The blood flow rate of 0.0625 mL/min was selected to correspond to 1 dyn/cm^2 shear stress based on the modeling.

Gas exchange testing of transwells was performed by pumping anticoagulated sheep blood (1% heparin; Lampire Biologics) with a syringe pump through the channel adjacent to the membrane of the transwell with oxygen flowing into and out of the top of the transwell (100 mL/min). Blood gas analysis was performed on the flowing blood before and after flowing past the transwell using a blood gas analyzer (Rapidlab 840; Chiron Diagnostics). $n=3$ per condition.

Manufacture of multi-channel gas exchange devices

Multi-channel gas exchange devices consisted of three PDMS layers: a square-channel vascular layer, an air chamber layer, and a lid (Fig. 1A). The vascular and air chamber layers were designed in SolidWorks (SolidWorks), and photolithography molds of these layers were produced on 10-cm silicon wafers (Stanford Microfluidics Foundry) and duplicated as polyurethane molds using Smooth-Cast 300 (Smooth-On). The vascular and air chamber layers were cast using standard soft lithography techniques. Air chamber layers were processed by using a scapel to introduce a beveled edge to the air chamber proper to increase media-holding capacity for cell culture without increasing the fixed gas exchange interface distance. Lids were cast from a 10-cm tissue culture dish lid.

Each device was divided into four ''quads,'' each with an independent blood input and output, operated separately and treated as independent samples. Within each quad, a series of 1:4, 1:4, and 1:6 channel branchings produced 96 100×100 μm square ''capillaries.'' The air chamber was oriented orthogonally to the direction of the blood flow, interfacing with the capillaries below *via* the collagen membrane.

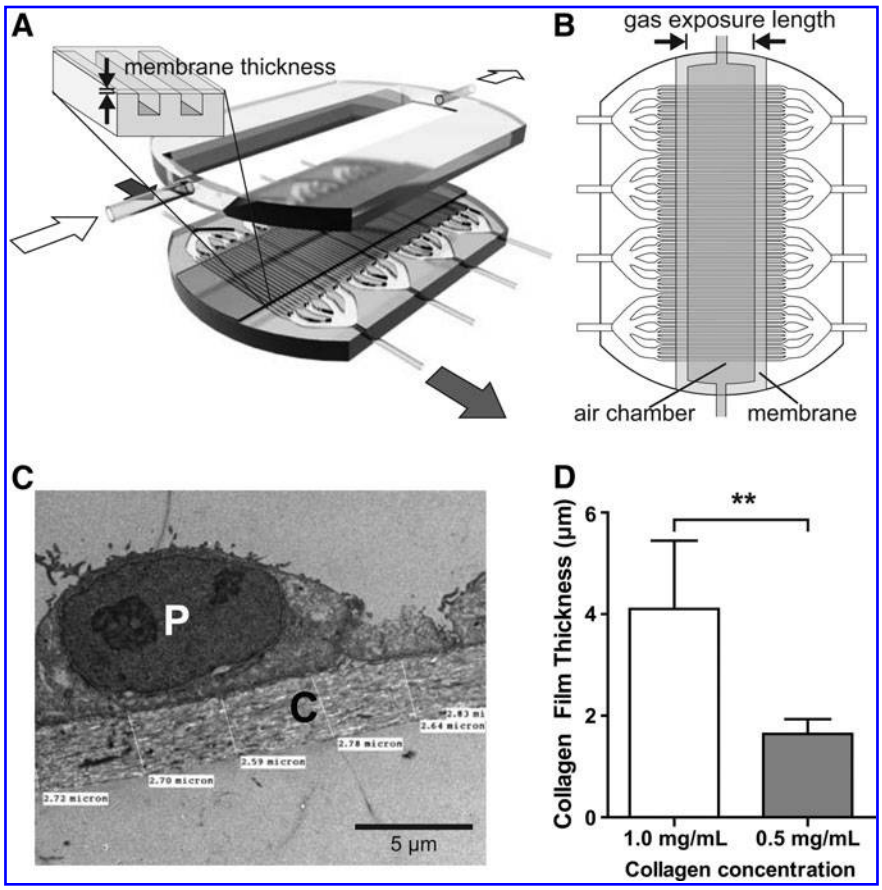

FIG. 1. Overview of multi-channel collagen-membrane gas exchange devices. **(A)** Three-dimensional schematic of a multi-channel collagen-membrane device, showing the assembly of the lower channel layer, collagen membrane, and parenchymal/air chamber layer. Blood flow is indicated by the *dark arrows*; airflow is indicated by the *light arrows*. Blown-up detail shows orientation of the collagen membrane and vascular channels (channels not to scale). **(B)** Overhead schematic of vascular channels with overlaid collagen membrane and air chamber to demonstrate alignment (channels not to scale). **(C)** Transmission electron microscopy (TEM) showing detail of collagen membrane [C] in tissue-engineered alveolus with A549 lung carcinoma cell [P]. **(D)** Comparison between thicknesses of collagen membranes produced using different collagen concentrations. $^{**}p < 0.01$.

Collagen films separating the capillaries and air chamber were produced using a modified protocol based on Vernon *et al.*[18] Rat collagen I (BD Biosciences) was diluted in $1\times$Dulbecco's modified Eagle's medium (DMEM) saturated with sodium bicarbonate, and pH was adjusted to 7.5 with NaOH. To spatially constrain the collagen membrane over the designated gas exchange region (Fig. 1A, B), a PDMS mask with a rectangular slit (20 or 13 mm wide for the 10 and 3 mm air chambers, respectively) (Fig. 1B) was overlaid atop the PDMS vascular layer, and the assembly was treated with oxygen plasma for 5 s at 100 W (Model PX-250; March Plasma Systems). Following removal of the mask, edges of the vascular layer bounding the channels on either side were trimmed to prevent collagen spillover along hydrophilic edges.

The collagen membrane was synthesized *in situ* over the vascular layer by pipetting the collagen solution onto the channel side of the device and allowing it to gel at 37°C. The prior selective plasma treatment defined a fixed hydrophilic region on the vascular channels, allowing reproducible dimensions of these membranes. Salts and dye were extracted by submerging the device in distilled water, and then the film was allowed to dessicate completely. During this process, the membrane becomes taut across the channels, forming the fourth wall of a closed rectangular channel rather than lining the bottom.

Finally, devices were assembled by bonding the air chamber layer atop the vascular layer *via* oxygen plasma activation for 10 s at 100 W. Air inlets on either side of the device, and four pairs of blood inlets and outlets, were generated by boring channels with a tissue biopsy punch and affixing silicone tubing with RTV silicone glue, with luer-lock fittings to interface with syringes for cell seeding and the gas exchange setup. All devices were sterilized by ethylene oxide before use.

Cell culture on multi-channel gas exchange devices

HUVECs were cultured in EGM-2 media (Lonza) and then seeded into vascular channels at $2–5\times10^6$ cells/mL ($\sim$200 µL per quad). The air chamber was filled with EGM-2 media, and inverted devices were incubated in standard tissue culture conditions for 1 h to promote attachment to the collagen membrane.

A549 cells were introduced into the upper chamber of the device at 1×10^5 cells/mL in a total of $\sim$10 mL DMEM with 10% fetal bovine serum, 100 U/mL penicillin, and 100 µg/mL streptomycin, and the devices were subsequently incubated for several days in the upright orientation until both cell populations reached confluency. All media in the air chamber was drained and replaced with ambient air before gas exchange testing.

Gas exchange testing of multi-channel collagen-membrane devices

Whole sheep's blood was aliquoted into capped 60-mL syringes and incubated at 37°C overnight to approximate gas content of venous blood in accordance with the guidelines for baseline blood parameters set forth in ISO 7199 for blood oxygenator testing.[19] Following incubation, the average

baseline values were as follows: SpO_2 70%; pCO_2 48 mmHg (6.4 kPa); hemoglobin: 10.1 g/dL.

The experimental setup is depicted in Figure 2A. About 0.1 L/min of 100% oxygen was bubbled through a humidifying column, then introduced into the air chamber, flowing orthogonally over all vascular channels before exiting to ambient air. The device was infused with blood using a syringe pump (PHD 2000; Harvard Apparatus), with the blood input flowing through gas-impermeable PVC tubing. Because of the thickness of the PDMS walls bounding the noncollagen sides of the channels, we calculated that the contribution of gas transmission through these walls to the total gas exchange is negligible. Tubing and devices were enclosed in an incubator to maintain the temperature at 37°C (Hybaid HS9320; Fisher Scientific). Baseline measurements were drawn from a three-way valve immediately upstream of the device, while experimental measurements were taken from a valve connected to the output tubing, with no opportunity for further gas exchange after the blood exited the vascular bed. Blood gases, pH, hematocrit, and bicarbonate levels were measured immediately upon sample acquisition using a Stat Profile Critical Care Xpress 12 (Nova Biomedical).

Transmission electron microscopy

Membranes were extracted from the devices and fixed in 2% glutaraldehyde. Imaging of cross sections was performed by the PMB Microscopy Core at Massachusetts General Hospital.

Immunofluorescence

Following 2–3 days in culture, cells were stained *in situ* on the membranes using anti-CD31 antibody (clone TLD-3A12; Millipore) at 10 μg/mL, phalloidin (Alexa Fluor 568 phalloidin; Invitrogen), and Hoechst.

Data analysis and statistical testing

Data were tabulated and analyzed in Excel (Microsoft Corp.), and statistical analysis and plotting was performed in GraphPad Prism (GraphPad Software, Inc.). For two-way ANOVA analysis in Figures 2 and 3, Bonferroni post-tests were conducted in two ways: first, comparing the four configurations against each other within each flow rate (significant differences are indicated in the figures, and all omitted relationships are nonsignificant), and second, comparing different

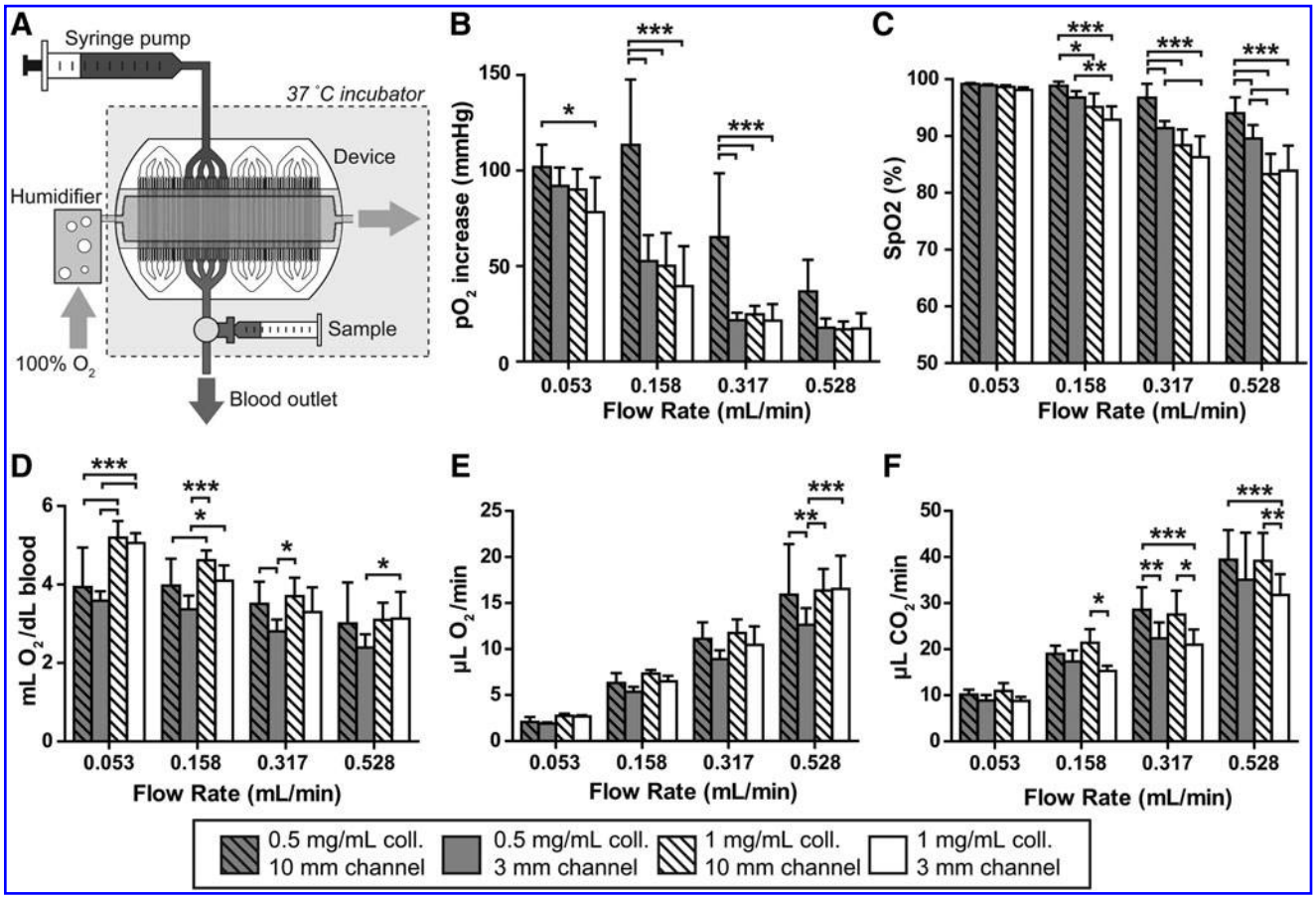

FIG. 2. Gas exchange in acellular multi-channel collagen-membrane devices. **(A)** Schematic representation of the gas exchange setup for testing both acellular and cellularized straight-channel devices. **(B)** Oxygenation as a function of flow rate, membrane thickness, and channel length, as measured by increase in partial pressure of oxygen. **(B–F)**, $*p<0.05$, $**p<0.01$, $***p<0.001$ by two-way ANOVA with Bonferroni post-test comparing configurations within each group **(C)** Hemoglobin oxygen saturation (%) as a function of flow rate, membrane thickness, and channel length. **(D)** Oxygen transfer per deciliter of blood. **(E)** Oxygen transfer per unit time. **(F)** Carbon dioxide clearance per unit time.

flow rates against each other within each configuration (for clarity, these significant differences are *not* indicated in the figures, but are noted in the text).

Results

We set out to design blood gas exchange devices centered on gas exchange across thin collagen membranes, hypothesizing that such membranes would not only recapitulate efficient gas exchange as seen in alveolar membranes, but also serve as a malleable substrate for relevant cell populations. As a demonstration of the feasibility of integrating cellularized collagen membranes into microfluidic devices for blood gas exchange, we first designed a prototype using a collagen membrane mounted on a transwell (Supplementary Fig. S1A). We seeded HUVECs and ''parenchymal'' cells (H441 lung adenocarcinoma cell line) on opposite sides of the membrane to mimic the sequence of cells found in the native alveolar blood-air interface (Supplementary Fig. S1B). To examine whether such adherent cells may remodel the collagen substrate in the context of these devices *in vitro*, we compared the thicknesses of membranes in tissue-engineered alveoli when incubated with media alone versus cultured with HUVECs and H441 cells. After 14 days, we measured a statistically significant 31% reduction in collagen film thickness in the presence of cells (Supplementary Fig. S1C, left), determined by transmission electron microscopy (TEM) (Supplementary Fig. S1C, right). To establish the practical impact of the presence of cells and change in film thickness, we affixed the tissue-engineered transwells on a single PDMS microfluidic channel such that the endothelial side directly formed the top of the channel and the parenchymal layer was in direct contact with air in the transwell chamber (Supplementary Fig. S1A). We then measured oxygen exchange by flowing sheep's blood at 0.0625 mL/min through the vascular channel and pure oxygen at 0.1 L/min through the air chamber (Supplementary Fig. S1D). pO_2 increases were comparable between the acellular collagen, endothelial cells-on-collagen, and fibroblasts-on-collagen controls, whereas seeding with both endothelial and ''parenchymal'' cells led to a statistically significant improvement in oxygenation. Together, these results established that thin collagen films can function as gas exchange membranes and support bifacial cell cultures, which in turn interact with and reconfigure the membrane.

Based on these initial insights, we designed and manufactured multi-channel collagen-membrane gas exchange devices that would allow us to rigorously quantify the impact of membrane thickness, gas exposure length, and flow rate on gas exchange. The devices contained four independent PDMS vascular beds (''quads''), each comprised of a vascular tree branching into 96 parallel channels that interface with a common air chamber *via* a large, contiguous collagen membrane (Fig. 1A). The geometric layout of channel branching and cross-sectional dimensions were based on prior designs and modeling, in which vascular networks with physiologic hemodynamics and efficient gas transfer were tested in the context of lung assist devices that employed thin, acellular silicone membranes.[16] For our new collagen-membrane devices, we used channels with 100×100 μm square cross sections, since in previous studies, larger channels (150×150 μm) were too deep to achieve full saturation during gas exchange, while shallower channels were less efficient due to lower throughput capacity.[16]

To explore the design space, we created device configurations with different gas exposure lengths at the fluid-air interface (3 mm vs. 10 mm, defined in Fig. 1B) and different thicknesses of collagen membranes as governed by the concentration of collagen in the collagen gel before dessication (1.0 mg/mL vs. 0.5 mg/mL). The gas exposure lengths were calculated to allow for blood traversal times on the order of 1 s at flow rates of interest, roughly corresponding to lung capillary gas exposure durations.[20] Recognizing that the magnitude of oxygen transfer in the single-channel transwell prototype was fairly modest, and hypothesizing that this result could be in part due to the thickness of the collagen membrane, we aimed to synthesize collagen membranes approximately an order of magnitude thinner than in the transwells. As measured by TEM on cross sections of several collagen membranes (Fig. 1C), film thickness was proportional to the collagen concentration in the cases tested, with 1.0 and 0.5 mg/mL gels yielding ~ 4 and ~ 2 μm membranes, respectively (Fig. 1D). These selected thicknesses were approximately informed by the human alveolus, where the gas exchange membranes are ~ 0.4–2 μm thick.[20,21]

We tested the gas exchange capacity of these acellular collagen-membrane devices using the experimental assembly depicted in Figure 2A: whole blood with typical venous oxygen and carbon dioxide content (average SpO_2 70%, pCO_2 48 mmHg) was pumped steadily into the devices' channels at flow rates of 0.0528, 0.1584, 0.3168, or 0.528 mL/min/quad while humidified oxygen flowed through the air chamber at a rate such that the oxygen concentration would not be meaningfully affected by gas exchange. The blood flow rates were determined based on approximate normal physiologic limits of shear stress, with the highest flow rate corresponding to 50 dyn/cm^2, a figure based on the range of shear stresses experienced by endothelial cells in human arteries and far below the shear limit of erythrocytes.[22,23] The flow rate to shear stress correspondence and the number of quads tested for each physical configuration at these blood flow rates are recorded in Table 1. For each condition, we measured the partial pressures of oxygen (pO_2) and carbon dioxide (pCO_2), oxygen saturation (SpO_2), bicarbonate, total CO_2, hemoglobin concentration, and pH.

The 0.5 mg/mL membrane/10 mm exposure length quads showed significantly larger increases in oxygen tension compared with the other three conditions in two of the flow rates tested ($p < 0.001$ by two-way ANOVA with Bonferroni post-test comparing configurations within each flow rate) (Fig. 2B). Additionally, all device configurations trended toward greater increases in pO_2 with slower flow rates.

Because the principal contributor to oxygen content in blood is the level of hemoglobin oxygen saturation, rather than freely dissolved oxygen, we also compared the configurations in terms of the oxygen saturation of blood exiting the device, drawn directly from gas-impermeable tubing at the device's outlets to preclude extraneous contact between the blood and ambient air. At the most rapid flow rate, saturation was lowest in the two thicker membrane conditions and highest in the 0.5 mg/mL membrane/10 mm exposure length configuration, in keeping with intuition

(Fig. 2C). Overall, regardless of membrane parameters, complete oxygen saturation (99–100%) was observed at the slowest flow rate while increases in flow rate led to diminishing saturation.

To integrate the hemoglobin-bound and dissolved oxygen measurements, the total oxygen content (mL O_2/dL blood) was computed from the following formula:[24]

$$O_2\ content = 1.34\left(\frac{mL\ O_2}{g}\right)\times \mathrm{Hgb}\left(\frac{g}{dL}\right)\times SpO_2 + 0.003\frac{mL}{mmHg}\times pO_2(mmHg)$$

As anticipated, the oxygen content of the exiting blood showed similar trends to the oxygen saturation (Fig. 2D). The total oxygen transfer rate (mL/min) was then calculated from these values and the blood flow rate as follows:

$$O_2\ transfer\ rate = Flow\ rate\times(output\ blood\ O_2\ content - baseline\ blood\ O_2\ content)$$

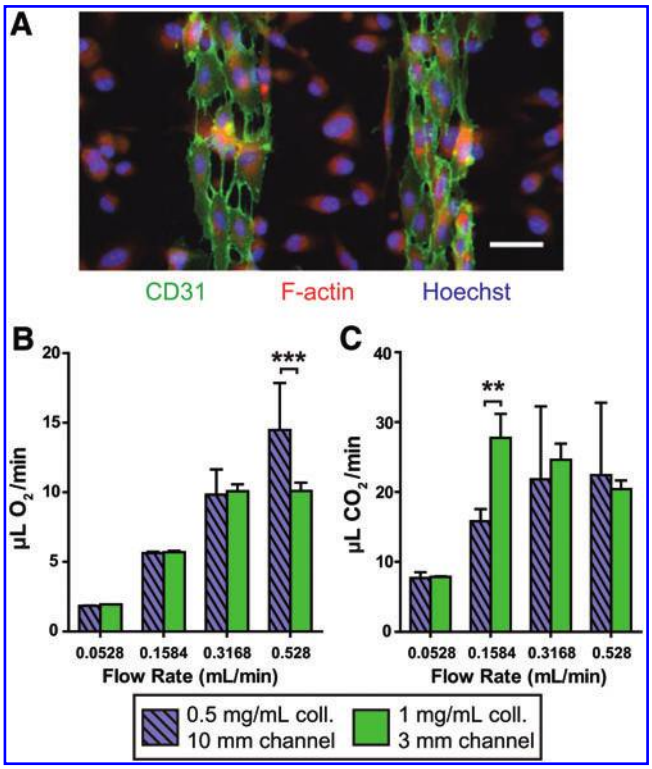

FIG. 3. Cellularized multi-channel collagen-membrane devices. **(A)** Immunocytochemical stain showing coculture of endothelial cells and lung epithelial cells, partway through the culturing process. *Green,* CD31; *red*, F-actin; *blue,* nuclei. Scale bar: 50 µm. **(B)** Oxygen transfer per unit time in devices cultured with human umbilical vein endothelial cells in the channels and A549 parenchymal cells in the air chamber. For **(B, C)**, $*p<0.05$, $**p<0.01$, $***p<0.001$ by two-way ANOVA with Bonferroni post-test comparing configurations within each group **(C)** Carbon dioxide clearance per unit time in devices with cell coculture as in **(B)**. Color images available online at www.liebertpub.com/tea

Table 1. Number of Quads Tested at Each Set of Parameters (Blood Flow Rate, Collagen Membrane Concentration, and Gas Exposure Length)

	0.0528	0.158	0.317	0.528	Flow rate (mL/min/quad)
	5	15	30	50	Shear stress (dyn/cm^2)
1 mg/mL, 3 mm	9	9	9	9	
1 mg/mL, 10 mm	6	6	6	6	
0.5 mg/mL, 3 mm	10	10	10	10	
0.5 mg/mL, 10 mm	11	11	10	9	

This metric, which quantified the functional efficiency of the device, revealed the significant impact of increasing blood throughput on the overall gas-exchange capacity of the collagen-membrane lung devices (Fig 2E). The oxygen transfer normalized to total membrane surface area, including collagen spanning inter-channel walls, ranged from 33 to 46 mL/min/m^2 at the minimal flow rate of 0.0528 mL/min to 220–288 mL/min/m^2 at the maximal flow rate of 0.528 mL/min. In addition to oxygen-related parameters, we also measured the changes in partial pressure of carbon dioxide (pCO_2), plasma bicarbonate, and total CO_2 in the same samples. The carbon dioxide clearance per unit time displayed the same trends as oxygenation but with higher magnitude across-the-board, in accordance with the higher rate of diffusion of carbon dioxide versus oxygen (Fig. 2F). The carbon dioxide transfer ranged from 153 to 190 mL/min/m^2 at the minimal flow rate of 0.0528 mL/min to 553–685 mL/min/m^2 at the maximal flow rate of 0.528 mL/min.

While acellular collagen-membrane lung devices represent an important step toward biomimetic design, the incorporation of cellular components is an important step toward future goals of both avoiding thrombogenicity and maintaining the integrity of the collagen membrane in the long term. Analogous to the single-channel transwell devices, we cultured endothelial cells (HUVECs) and ''parenchymal'' cells (A549) on opposite sides of the collagen membrane, facing the vascular channels and air chamber, respectively. We confirmed the presence of both cell types *via* immunofluorescent staining for CD31 (endothelial cell junctions) and F-actin (any cell cytoplasm) as shown in Figure 3A, which depicts a partially-confluent cellularized collagen membrane during the culture process; a confluent parenchymal cell layer is shown in Supplementary Fig. S2A. To ensure that cells would not be dislodged by the presence of flow in the channels, we seeded endothelial cells in the device channels as before; after they had adhered, we subjected them to media flowing at 0.5 mL/min/quad for a period of 3 h, confirming through immunofluorescence that the endothelial layer remains intact on the collagen membrane (Supplementary Fig. S2B).

We then performed gas exchange testing on two of the original four configurations as cellular devices: 1 mg/mL collagen with 3 mm channel length ($n=5$) and 0.5 mg/mL collagen with 10 mm channel length ($n=3$). The rates of oxygen and carbon dioxide transfer in cellularized devices (Fig. 3B, C) were comparable to those in acellular devices, but notably, the oxygenation was not significantly different

between the two fastest flow rates, and carbon dioxide release was not significantly different among the three highest flow rates.

Discussion

Our results establish the feasibility of using ultra-thin collagen membranes in gas exchange devices. The type I collagen membranes that we tested were easily colonized by endothelial and epithelial cells in a configuration mimicking the native alveolus, demonstrated by the bifacial seeding of representative cell populations in the tissue-engineered alveolus devices (Supplementary Fig. S1B). Moreover, these membranes were extensively remodeled by adherent cells, producing thinner membranes (Supplementary Fig. S1C). In our multi-channel devices, the membranes were as thin as 2 μm, approaching the normal range of the human alveolar-capillary barrier ($\sim$0.4–2 μm). Furthermore, the generalized method of producing such membranes could be easily tailored to test varying compositions of ECM in the future to support cell attachment and differentiation.

The key metric of performance for any artificial lung device is gas exchange: blood oxygenation and carbon dioxide clearance. At the highest flow rate, the acellular multi-channel devices exhibited excellent oxygen exchange efficiency: up to 16.5 μL O_2/min on a surface area of 57.5 mm^2 per quad, or 288 mL/min/m^2 of membrane. This compares favorably against the previous generation of lung devices from our lab, which achieved 34 mL/min/m^2,[25] and approaches the native human lung, which transfers oxygen at 21–65 mL/min per mmHg of oxygen gradient[26] over a $\sim$70 m^2 surface area, for an efficiency of $\sim$217–672 mL/min/m^2 on pure oxygen. Because the output oxygen saturation–and thus total oxygen transferred per deciliter of blood–was only moderately decreased by the flow rate, the oxygen transfer rate per unit time always increased with increasing blood flow rates (Fig. 2E). Importantly, for these studies, we capped flow rates at physiologic arterial shear stresses, but it is likely that an endothelial cell layer would tolerate higher flow rates that could correspond to further increases in oxygen transfer.

Although the oxygen transfer in these devices was excellent, we observed scenarios in which the output blood was not fully saturated and the pO_2 did not reach the ideal of at least 100 mmHg, reflecting the net influence of channel depth, membrane properties, and flow rate on the devices' performance. In the acellular collagen-membrane devices, we observed a general trend toward greater increases in ΔpO_2 at slower flow rates, regardless of collagen membrane thickness or residence time, ranging from $\sim$20 mmHg at 0.528 mL/min/quad to $\sim$100 mmHg at 0.0528 mL/min/quad (Fig. 2B). The configuration with the thinnest membrane and longest gas exposure distance showed the greatest magnitude of ΔpO_2 at all flow rates, with statistically significant differences versus the other configurations at all but the fastest blood flow rate. This result agrees with the hypothesized impact of thinning the membrane or lengthening the exchange tract and argues for the importance of working with ultra-thin collagen membranes that approach the thinness of the alveolar gas exchange barrier.

At the highest flow rates tested in our study, the blood output reached oxygen saturations in the 80–95% range rather than full saturation (Fig. 2C), suggesting that there is still room for device optimization. As with the ΔpO_2 data, the effect was most pronounced with the thicker membrane and shorter gas exposure distance conditions, but in all configurations, the oxygen saturation at the 0.0528 mL/min flow rate was statistically significantly better than the saturation at the 0.528 mL/min flow rate ($p < 0.001$ by two-way ANOVA with Bonferroni post-test comparing across flow rates).

One strategy for addressing incomplete saturation without further thinning the membrane or lengthening the channel is to reduce the channel size: We have previously shown that if the channel size is decreased below 100 μm, the oxygen saturation improves at higher flow rates.[16] As such, one contributing factor to the incomplete hemoglobin saturation at faster flow rates may be the laminar flow in these straight, narrow, 1:1 aspect ratio channels, where minimal mixing is preferable for reducing the risk of thrombus formation but less amenable to facilitating gas exchange. The optimal channel size is not yet understood but must balance (1) achieving optimal hemoglobin saturation, (2) allowing ample blood flow rate so that a device with practical oxygenation capacity remains a reasonable size, and (3) minimizing the risk of thrombus formation. Cellularization of the devices, including the gas exchange membrane as shown in this work but ideally encompassing all sides of the vessels, may modulate the correspondence between channel size and risk of thrombosis. Without endothelial cells, the smallest channel size that corresponds to a minimal risk of device thrombosis with therapeutic anticoagulation may be 100 μm or even larger. Endothelialization of the devices would provide the best natural barrier to thrombus formation and may allow the channel size to decrease below 100 μm. Native capillaries in the lung are less than 10 μm in diameter, and although this is theoretically achievable, it may be more reasonable to consider endothelialized microchannels on the range of 25–50 μm in diameter as feasible to achieve without thrombosis, particularly because larger channels are preferable for minimizing space occupied by scaffolding.

Despite these observations of incomplete saturation, the data overall remain most consistent with the oxygenation process being blood perfusion-limited rather than oxygen diffusion-limited, similar to the situation in native lungs, which are only diffusion-limited in the case of extreme physical exertion or diseased states.[20] While diffusion-limited devices would be expected to show approximately constant oxygen transfer rates at all flow rates, with oxygen transfer per unit volume of blood dropping off as flow rates increase, the multi-channel collagen-membrane devices instead showed increasing oxygen transfer rates (Fig. 2E) and fairly steady oxygen transfer per unit volume (Fig. 2D) with increasing flow rate. Indeed, over the flow rates tested, the oxygen transfer rate (Fig. 2E) as a function of perfusion can be closely approximated with linear regression through the origin, with R^2 of 0.92–0.97 for all configurations. In the future, greater oxygen transfer efficiency may be achieved by further increasing flow rates, limited only by the shear tolerance of endothelial cells.

In addition to blood oxygenation, carbon dioxide clearance from blood is also centrally important for lung devices. The trends in carbon dioxide transfer mirrored those in oxygen transfer, with absolute volumes about twice as large (Fig. 2F).

The carbon dioxide clearance is adequate to lower pCO_2 into the normocapnic range, even at the highest flow rates (data not shown). In keeping with the efficient O_2 gas transfer on a per-area basis, the maximal CO_2 transfer achieved with the collagen membrane devices was 685 mL/min/m^2. These higher CO_2 transfer rates are similar to what we have observed with silicone membranes in a microchannel-based lung device[25] and are consistent with the native lung, which also exhibits higher maximal CO_2 transfer rates.

The cellularized devices yielded similar magnitudes of oxygen and carbon dioxide transfer per minute compared to the acellular devices, peaking at around 10 μL/min O_2 and 20 μL/min CO_2 (Fig. 3B, C). Interestingly, there were not significant differences between the two highest blood flow rates for oxygen transfer in either cellularized configuration, implying diffusion limitation in this regime. The diffusion limitation may be related to the membrane and associated cells, diffusion through the entire depth of the channel, or likely a combination of both. This finding may also reflect the limitations of our model cell lines, as the inherent thickness of A549 cells compared to healthy primary pneumocytes may impede effective gas exchange as compared to the bare membrane or a membrane lined with flat epithelium. It is thus possible that use of more phenotypically stable, differentiable cells such as neonatal lung epithelial cells or iPS-derived alveolar epithelial cells may reconcile the cellular device data with the acellular data.

The blood gas exchange results for cellularized devices serve as a first step toward harnessing the potential of cellularization to improve long-term durability of collagen membranes and reduce thrombogenicity. Experiments relating to these hypotheses (such as long-term perfusion followed by imaging of thrombus deposition, platelet adhesion studies, and staining to assess endothelial cell activation state) could not be tested in the current device design, since the present membrane only comprises one of the four walls of the square channels. As such, comparisons to existing technologies regarding durability and biocompatibility cannot be made at this time. However, alternative methods of collagen patterning and deposition could produce channels wholly comprised of collagen, enabling future blood biocompatibility studies; furthermore, long-term durability may be tested with differentiated cells that would not overgrow after reaching a confluent layer.

In summary, we have designed and tested collagen membrane-based lung assist device prototypes that exhibit favorable oxygen and carbon dioxide exchange capacity. The membrane readily supports adherent endothelial and parenchymal cells, which are able to remodel the membrane. We envision that incorporation of biologically-inspired gas exchange interfaces, in conjunction with advancements in microfluidic device design, may ultimately yield efficient, biocompatible lung devices that can supplement native lungs in patients with chronic lung disease.

Acknowledgments

The authors gratefully acknowledge support from the NIH (F32 DK076349-01, DMH) and NIH/NIGMS (MSTP T32GM007753, JHL). The authors would like to thank Baoling Liu, Yongqing Li, *et al.* for use of their blood analyzer, Mary McKee at the PMB Microscopy Core at Massachusetts General Hospital for TEM imaging, and Jessica Melin and the Stanford Microfluidics Foundry for fabrication of the microfluidic molds. The content is solely the responsibility of the authors and does not necessarily represent the official views of the National Institute of General Medical Sciences or the National Institutes of Health.

Disclosure Statement

No competing financial interests exist.

References

1. Minino, A.M., Murphy, S.L., Xu, J., and Kochanek, K.D. Deaths: final data for 2008. Natl Vital Stat Rep **59,** 1, 2011.
2. Kozower, B.D., Meyers, B.F., Smith, M.A., De Oliveira, N.C., Cassivi, S.D., Guthrie, T.J., Wang, H., Ryan, B.J., Shen, K.R., Daniel, T.M., and Jones, D.R. The impact of the lung allocation score on short-term transplantation outcomes: a multicenter study. J Thorac Cardiovasc Surg **135,** 166, 2008.
3. Fischer, S., Hoeper, M.M., Tomaszek, S., Simon, A., Gottlieb, J., Welte, T., Haverich, A., and Strueber, M. Bridge to lung transplantation with the extracorporeal membrane ventilator Novalung in the veno-venous mode: the initial Hannover experience. ASAIO J **53,** 168, 2007.
4. Mateen, F.J., Muralidharan, R., Shinohara, R.T., Parisi, J.E., Schears, G.J., and Wijdicks, E.F. Neurological injury in adults treated with extracorporeal membrane oxygenation. Arch Neurol **68,** 1543, 2011.
5. Lund, L.W., and Federspiel, W.J. Removing extra CO_2 in COPD patients. Curr Respir Care Rep **2,** 131, 2013.
6. Bartosik, W., Egan, J.J., and Wood, A.E. The Novalung interventional lung assist as bridge to lung transplantation for self-ventilating patients—initial experience. Interact Cardiovasc Thorac Surg **13,** 198, 2011.
7. Huh, D., Leslie, D.C., Matthews, B.D., Fraser, J.P., Jurek, S., Hamilton, G.A., Thorneloe, K.S., McAlexander, M.A., and Ingber, D.E. A human disease model of drug toxicity-induced pulmonary edema in a lung-on-a-chip microdevice. Sci Transl Med **4,** 159ra147, 2012.
8. Huh, D., Matthews, B.D., Mammoto, A., Montoya-Zavala, M., Hsin, H.Y., and Ingber, D.E. Reconstituting organ-level lung functions on a chip. Science **328,** 1662, 2010.
9. Lee, J.K., Kung, H.H., and Mockros, L.F. Microchannel technologies for artificial lungs: (1) theory. ASAIO J **54,** 372, 2008.
10. Lee, J.K., Kung, M.C., Kung, H.H., and Mockros, L.F. Microchannel technologies for artificial lungs: (3) open rectangular channels. ASAIO J **54,** 390, 2008.
11. Sugihara, H., Toda, S., Miyabara, S., Fujiyama, C., and Yonemitsu, N. Reconstruction of alveolus-like structure from alveolar type II epithelial cells in three-dimensional collagen gel matrix culture. Am J Pathol **142,** 783, 1993.
12. Zhang, W.J., Lin, Q.X., Zhang, Y., Liu, C.T., Qiu, L.Y., Wang, H.B., Wang, Y.M., Duan, C.M., Liu, Z.Q., Zhou, J., and Wang, C.Y. The reconstruction of lung alveolus-like structure in collagen-matrigel/microcapsules scaffolds in vitro. J Cell Mol Med **15,** 1878, 2011.
13. Petersen, T.H., Calle, E.A., Zhao, L., Lee, E.J., Gui, L., Raredon, M.B., Gavrilov, K., Yi, T., Zhuang, Z.W., Breuer, C., Herzog, E., and Niklason, L.E. Tissue-engineered lungs for in vivo implantation. Science **329,** 538, 2010.
14. Ott, H.C., Clippinger, B., Conrad, C., Schuetz, C., Pomerantseva, I., Ikonomou, L., Kotton, D., and Vacanti, J.P.

Regeneration and orthotopic transplantation of a bioartificial lung. Nat Med **16,** 927, 2010.
15. Bonvillain, R.W., Danchuk, S., Sullivan, D.E., Betancourt, A.M., Semon, J.A., Eagle, M.E., Mayeux, J.P., Gregory, A.N., Wang, G., Townley, I.K., Borg, Z.D., Weiss, D.J., and Bunnell, B.A. A nonhuman primate model of lung regeneration: detergent-mediated decellularization and initial in vitro recellularization with mesenchymal stem cells. Tissue Eng Part A **18,** 2437, 2012.
16. Bassett, E.K., Hoganson, D.M., Lo, J.H., Penson, E.J., and Vacanti, J.P. Influence of vascular network design on gas transfer in lung assist device technology. ASAIO J **57,** 533, 2011.
17. Hess, C., Wiegmann, B., Maurer, A.N., Fischer, P., Moller, L., Martin, U., Hilfiker, A., Haverich, A., and Fischer, S. Reduced thrombocyte adhesion to endothelialized poly 4-methyl-1-pentene gas exchange membranes-a first step toward bioartificial lung development. Tissue Eng Part A **16,** 3043, 2010.
18. Vernon, R.B., Gooden, M.D., Lara, S.L., and Wight, T.N. Native fibrillar collagen membranes of micron-scale and submicron thicknesses for cell support and perfusion. Biomaterials **26,** 1109, 2005.
19. ISO. ISO 7199: Cardiovascular implants and artificial organs—Blood-gas exchangers (oxygenators). Geneva, Switzerland: ISO, 2009.
20. Koeppen, B.M., and Stanton, B.A. Berne & Levy Physiology. 6th ed. Philadelphia, PA: Mosby Elsevier, 2008.
21. Maina, J.N., and West, J.B. Thin and strong! The bioengineering dilemma in the structural and functional design of the blood-gas barrier. Physiol Rev **85,** 811, 2005.
22. Hoganson, D.M., Pryor, H.I., 2nd, Spool, I.D., Burns, O.H., Gilmore, J.R., and Vacanti, J.P. Principles of biomimetic vascular network design applied to a tissue-engineered liver scaffold. Tissue Eng Part A **16,** 1469, 2010.
23. Pappano, A.J., and Wier, W.G. Cardiovascular Physiology. 10th ed. Philadelphia, PA: Mosby, 2012.
24. Shimono, T., Shomura, Y., Hioki, I., Shimamoto, A., Tenpaku, H., Maze, Y., Onoda, K., Takao, M., Shimpo, H., and Yada, I. Silicone-coated polypropylene hollow-fiber oxygenator: experimental evaluation and preliminary clinical use. Ann Thorac Surg **63,** 1730, 1997.
25. Hoganson, D.M., Pryor, H.I., 2nd, Bassett, E.K., Spool, I.D., and Vacanti, J.P. Lung assist device technology with physiologic blood flow developed on a tissue engineered scaffold platform. Lab Chip **11,** 700, 2011.
26. Hall, J.E. Guyton and Hall Textbook of Medical Physiology. 12th ed. Philadelphia, PA: Saunders Elsevier, 2011.

Address correspondence to:
Joseph P. Vacanti, MD
Department of Surgery
55 Fruit St.
Massachusetts
General Hospital
Boston, MA 02114

E-mail: jvacanti@partners.org

Received: June 19, 2014
Accepted: March 31, 2015
Online Publication Date: July 15, 2015